SCIENCE CHINA
Chemistry

•ARTICLES•

https://doi.org/10.1007/s11426-023-1902-0

Enhancing the deep-red/near-infrared fluorescence of higher rylene diimides *via* the chalcogen-annulation strategy

Kai Chen[1], Xiao Chen[2], Ke Hu[3], Yilun Zhao[1], Yujian Liu[2], Guogang Liu[1*], Jinquan Chen[3], Wei Jiang[1,2], Zhigang Shuai[2], Da-Hui Qu[1] & Zhaohui Wang[1,2*]

[1]*Key Laboratory for Advanced Materials and Joint International Research Laboratory of Precision Chemistry and Molecular Engineering, Feringa Nobel Prize Scientist Joint Research Center, Frontiers Science Center for Materiobiology and Dynamic Chemistry, Institute of Fine Chemicals, School of Chemistry and Molecular Engineering, East China University of Science and Technology, Shanghai 200237, China;*
[2]*Key Laboratory of Organic Optoelectronics and Molecular Engineering, Department of Chemistry, Tsinghua University, Beijing 100084, China;*
[3]*State Key Laboratory of Precision Spectroscopy, East China Normal University, 500 Dongchuan Road, Shanghai 200241, China*

Received August 15, 2023; accepted December 15, 2023; published online January 5, 2024

Deep-red/near-infrared fluorescence is highly suitable for bioimaging owing to its ability to deeply penetrate tissues, organs, and live animals. However, developing organic fluorophores with high deep-red/near-infrared fluorescence quantum yield (Φ_{FL}) and fluorescent brightness remain a significant challenge owing to the energy gap law. Herein, we developed a straightforward and effective chalcogen-annulation strategy by introducing O, S and Se into the bay region of **TDI** and **QDI** fluorophores, realizing the increase of Φ_{FL} and fluorescent brightness up to 10 times. To our best knowledge, this study potentially stands as the pioneering instance showcasing the anti-heavy-atom effect of chalcogens, and the absolute Φ_{FL} (93%) and fluorescent brightness (128,200 cm^{-1} mol^{-1} L) of **Se-TDI** is among top deep-red/near-infrared organic fluorophores currently available. The femtosecond transient absorption (fs-TA) measurements show the absence of obvious changes of the excited state lifetime after the introduction of chalcogens in **TDI** and **QDI** fluorophores, indicating that intersystem crossing (ISC) can be neglected in TDI and QDI fluorophores. Theoretical calculations further reveal the chalcogen-annulation strategy increase the radiative rates and reduce the reorganization energy of several accepting modes at the ground state in **TDI** fluorophores, leading to the suppression of internal conversion (IC) processes. Our chalcogen-annulation strategy, which effectively increases the Φ_{FL} and restricts the IC processes, while remaining unaffected by the heavy-atom effect, offers novel insights and theoretical support for the design and synthesis of deep-red/near-infrared organic fluorophores with high Φ_{FL} and fluorescent brightness.

π-extended rylene diimides, chalcogen-annulation strategy, deep-red/near-infrared fluorescence

Citation: Chen K, Chen X, Hu K, Zhao Y, Liu Y, Liu G, Chen J, Jiang W, Shuai Z, Qu DH, Wang Z. Enhancing the deep-red/near-infrared fluorescence of higher rylene diimides *via* the chalcogen-annulation strategy. *Sci China Chem*, 2024, 67, https://doi.org/10.1007/s11426-023-1902-0

1 Introduction

In recent years, there has been an increasing emphasis on deep-red/near-infrared fluorescence in the field of bioimaging, owing to its exceptional capacity to penetrate organoids, tissues, organs, and live animals deeply while maintaining a high signal-to-background ratio [1–4]. Among the various deep-red/near-infrared materials, organic fluorophores are highly favored for their excellent derivatization, versatility, and well-established safety profile accumulated through years of clinical use [5–24]. However, developing deep-red/near-infrared organic fluorophores with high fluorescence quantum yield (Φ_{FL}) and fluorescent brightness

*Corresponding authors (email: liuguogang@ecust.edu.cn; wangzhaohui@mail.tsinghua.edu.cn)

(the product of molar extinction coefficient and Φ_{FL}, which is a crucial factor for enhancing imaging resolution) remains a significant challenge owing to the rapid internal conversion (IC) quenching processes, commonly known as the energy gap law [25].

Rylene diimides, a well-known class of polycyclic aromatic hydrocarbons, have garnered ever-increasing attention owing to their unique rigidly conjugated framework and excellent physicochemical properties, enabling their wide application in organic optoelectronic fields [26–43]. Among the rylene diimides family, perylene diimides (**PDI**) are renowned for their outstanding molar extinction coefficient (ε) and high Φ_{FL} in the visible-light region [44–46], making them highly sought-after in the field of bioimaging [47–50]. However, their counterparts, the longitudinal π-extended terrylene diimides (**TDI**) and quaterrylene diimides (**QDI**) fluorophores, which possess deep-red/near-infrared absorption/emission and higher ε values than **PDI** [51,52], suffer from a notable decrease in Φ_{FL} and fluorescent brightness. Although considerable progress have been made in synthetic and biological explorations concerning **TDI** and **QDI** fluorophores [53,54], achieving high deep-red/near-infrared Φ_{FL} and fluorescent brightness in **TDI** and **QDI** fluorophores remains a great challenge [55–59]. Nevertheless, recent reports have presented a growing body of evidence on organic fluorophores containing heavy atoms that exhibit an intriguing anti-heavy-atom effect, where the presence of heavy atoms enhances their Φ_{FL} and fluorescent brightness, contrary to conventional understanding [60–64]. Although the anti-heavy-atom effect of transition metals [61–66] and halogens [67–69] has been studied in a few instances in the literature, the potential anti-heavy-atom effect of chalcogens remains unexplored.

Herein, we successfully synthesized a series of **TDI** and **QDI** fluorophores through straightforward nitration and chalcogen-annulation in the bay region (Scheme 1). Our research revealed the chalcogen-annulation strategy can considerably enhance the deep-red/near-infrared Φ_{FL} and fluorescent brightness of **TDI** and **QDI** fluorophores up to 10 times (Figure 1a). It is in stark contrast with the decrease in Φ_{FL} and fluorescent brightness observed in the chalcogen-annulation of the PDI fluorophores (Figure 1b) [37]. To the best of our knowledge, this is the first example of the anti-heavy-atom effect observed with chalcogens (Φ_{FL}(**O-TDI**) < Φ_{FL}(**S-TDI**) < Φ_{FL}(**Se-TDI**)) and the Φ_{FL} (93%) and fluorescent brightness of **Se-TDI** (128,200 cm^{-1} mol^{-1} L) ranks among those of the top deep-red/near-infrared organic fluorophores available [70]. The time-resolved fluorescence lifetime and fs-TA experiment reveal that the fluorescence lifetimes are below 3.65 ns and the absence of obvious changes of the excited state lifetimes in **TDI** and **QDI** fluorophores. These results indicate that intersystem crossing (ISC) can be neglected in TDI and QDI fluorophores. Theoretical calculations further confirm these results and reveal the suppressing of internal conversion (IC) processes of **TDI** fluorophores by reducing the reorganization energy of several important accepting modes in the ground state (Figure 1c). Our chalcogen-annulation strategy, which effectively increases the Φ_{FL} and restricts the IC processes, while remaining unaffected by heavy-atom effect, offers novel insights and theoretical support for the design and synthesis of deep-red/near-infrared organic fluorophores with high Φ_{FL} and fluorescent brightness.

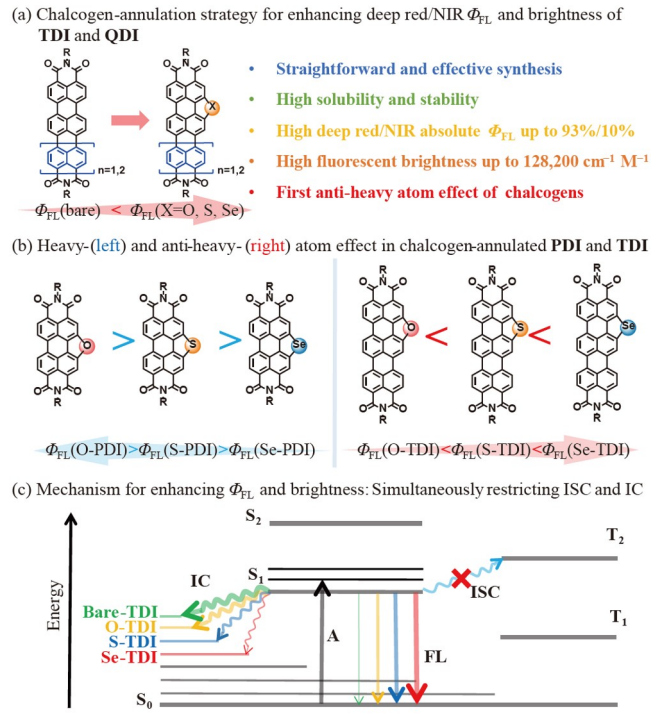

Figure 1 (a) Change rules in Φ_{FL} and fluorescent brightness of **TDI** and **QDI** fluorophores *via* chalcogen-annulation. (b) Heavy-atom and anti-heavy-atom effect in chalcogen-annulated **PDI** and **TDI**. (c) Jablonski diagram of energy conversion processes of **TDI** fluorophores (color online).

2 Results and discussion

2.1 Synthesis of chalcogen-annulated TDI and QDI

The choice of nitration reagents plays a crucial role in the nitration reaction, as **TDI** and **QDI** demonstrate high susceptibility to nitration (Scheme 1). The use of nitrating reagents such as nitric acid can lead to the formation of dinitro- and trinitro-products within a short timeframe, diminishing the yield of mononitro-products and complicating the separation process [71]. Through extensive experimentation with various nitrating reagents, we ultimately opted for a relatively mild nitration reagent, tert-butyl nitrite, for the nitration reaction. By fine-tuning the reaction conditions, we achieved impressive yields of up to 90% for both **NO_2-TDI**

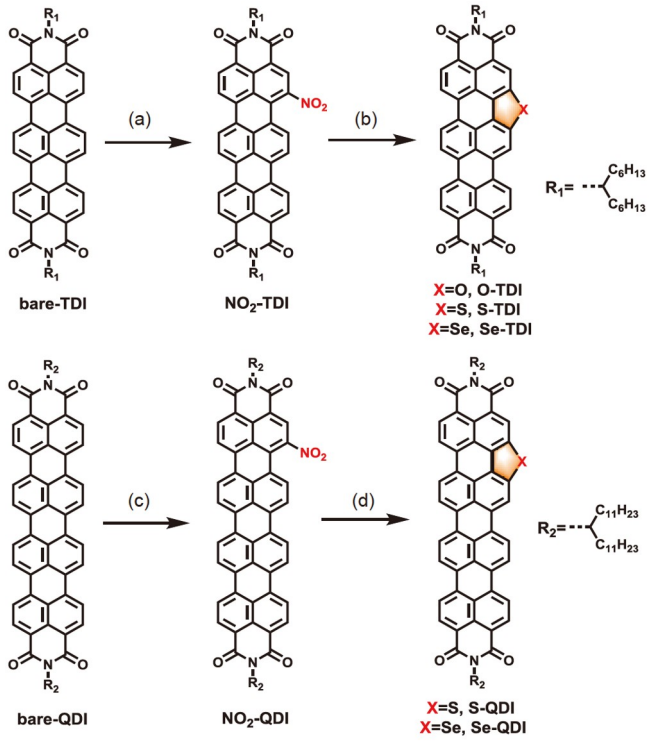

Scheme 1 Synthesis routes for **O-TDI**, **S-TDI**, **Se-TDI**, **S-QDI** and **Se-QDI**. (a) Tert-butyl nitrite, CH_2Cl_2, r.t., 4 h, 90%. (b) **O-TDI**: air, NMP, 190 °C, 12h, 15%; **S-TDI**: S powder, NMP, 190 °C,2 h, 60%; **Se-TDI**: Se powder, NMP, 190 °C,4 h, 50%. (c) Tert-butyl nitrite, $CHCl_3$, r.t., 4 h, 90%. (d) **S-QDI**: S powder, NMP, 190 °C,4 h, 50%; **Se-QDI**: Se powder, NMP, 190 °C,4 h, 50% (color online).

and **NO_2-QDI** using CH_2Cl_2 and $CHCl_3$ as solvents, respectively. The conditions for chalcogen-annulation reactions of **NO_2-TDI** closely resemble those of **NO_2-PDI** [37]. By employing *N*-methyl-2-pyrrolidone (NMP) as the solvent, air, S powder, and Se powder as the raw materials, we conducted the reactions at 180 °C for 12 h, 2 h, and 4 h, respectively. The yields of **O-TDI**, **S-TDI** and **Se-TDI** were 15%, 60%, and 50%, respectively. Using identical reaction conditions, we also successfully synthesized **S-QDI** and **Se-QDI**, both yielding 50%. Regrettably, our efforts to synthesize **O-QDI** were unsuccessful. The challenge stems from a notable decrease in reactivity observed in the annulation reaction between oxygen and longitudinally π-extended rylene diimides. This limitation might also account for the low yield of **O-TDI** at 15%, notably lower than the previously reported 30% yield for **O-PDI** [37]. The structures of **O-TDI**, **S-TDI**, **Se-TDI**, **S-QDI** and **Se-QDI** were unambiguously characterized using NMR and high-resolution mass spectra. These compounds have good solubility and stability in common organic solvents such as toluene, dichloromethane, tetrahydrofuran, dioxane and NMP.

2.2 Absorption, fluorescence and electrochemical properties

The ground-state electronic properties of **TDI** fluorophores were explored using steady-state absorption spectroscopy measurement in toluene at room temperature (Figure 2a–2d). **Bare-TDI**, **O-TDI**, **S-TDI** and **Se-TDI** exhibit electronic absorption spectra corresponding to the $S_0 \rightarrow S_1$ transition with well-resolved vibronic bands having absorption maxima at ($\lambda_{Abs\ max}$) 650 nm for **bare-TDI**, 638 nm for **O-TDI**, 624 nm for **S-TDI**, and 631 nm for **Se-TDI**. The $S_0 \rightarrow S_1$ electronic transition of **TDI** fluorophores is strongly coupled to the vinyl stretching mode of the **TDI** core, ensuring distinct vibronic progression in the absorption spectra (Figure 2a). The vibronic features are at 598 nm ($\lambda_{Abs\ 0-1}$) for **bare-TDI**, 589 nm ($\lambda_{Abs\ 0-1}$) for **O-TDI**, 576 nm ($\lambda_{Abs\ 0-1}$) for **S-TDI**, and 582 nm ($\lambda_{Abs\ 0-1}$) for **Se-TDI**. The hypsochromic shift of chalcogen-annulated **TDI** are 12, 26 and 19 nm with respect to **bare-TDI.** The variation pattern of the UV-vis-NIR absorption spectra of **QDI** fluorophores is very similar to that of **TDI** fluorophores, where the $\lambda_{Abs\ max}$ of **bare-QDI**, **S-QDI** and **Se-QDI** is 790 nm, 766 nm and 775 nm (Figure 2b), respectively. And their $S_0 \rightarrow S_1$ electronic transition is also strongly coupled to the vinyl stretching mode. And the vibronic features are at 685 nm ($\lambda_{Abs\ 0-1}$) for **bare-QDI**, 670 nm ($\lambda_{Abs\ 0-1}$) for **S-QDI**, and 676 nm ($\lambda_{Abs\ 0-1}$) for **Se-QDI**. The hypsochromic shift of **S-QDI** and **Se-QDI** is 24 and 15 nm with respect to **bare-QDI**.

Steady-state fluorescence spectroscopy measurements were performed to understand the photoluminescence properties of chalcogenide **TDI** and **QDI** fluorophores in toluene. The fluorescence spectra of **bare-PDI**, **O-TDI**, **S-TDI**, and **Se-TDI** exhibit mirror-image characteristics with their respective steady-state absorption spectra (Figure 2c). The fluorescence emission peaks are observed at 667 nm for **bare-TDI** (Stokes shift, $\Delta\nu'' \approx 392.1\ cm^{-1}$), 658 nm for **O-TDI** ($\Delta\nu'' \approx 476.4\ cm^{-1}$), 638 nm for **S-TDI** ($\Delta\nu'' \approx 351.7\ cm^{-1}$), and 645 nm for **Se-TDI** ($\Delta\nu'' \approx 344.0\ cm^{-1}$). According to the Franck–Condon principle, we can identify the distinct vibronic features in the fluorescence spectra ($\lambda_{Em\ 0-1}$) of **bare-TDI**, **O-TDI**, **S-TDI** and **Se-TDI** at 728 nm, 710 nm, 700 nm and 705 nm, respectively. These properties indicate that chalcogens-annulated **TDI** fluorophores are potential bioimaging dyes in deep-red regions. The fluorescence spectra of **QDI** fluorophores exhibit similar rigidity to **TDI** fluorophores, adhering to both the mirror-image rule and the Franck–Condon principle. The $\lambda_{Em\ max}$ and $\lambda_{Em\ 0-1}$ are at 790 nm and 860 nm for **bare-QDI**, 766 nm and 834 nm for **S-QDI**, 775 nm and 843 nm for **Se-QDI**, respectively (Figure 2d).

The absolute Φ_{FL} of **bare-TDI**, **O-TDI**, **S-TDI**, and **Se-TDI** was determined to be 72%, 79%, 90%, and 93% (Table 1), respectively. Additionally, the steady-state absorption spectra reveal that their corresponding maximal ε is 135,300, 127,700, 132,400 and 137,800 $mol^{-1}\ L\ cm^{-1}$, respectively. The progressive improvement of Φ_{FL}, combined with the relatively constant maximal ε, results in a gradual increase in

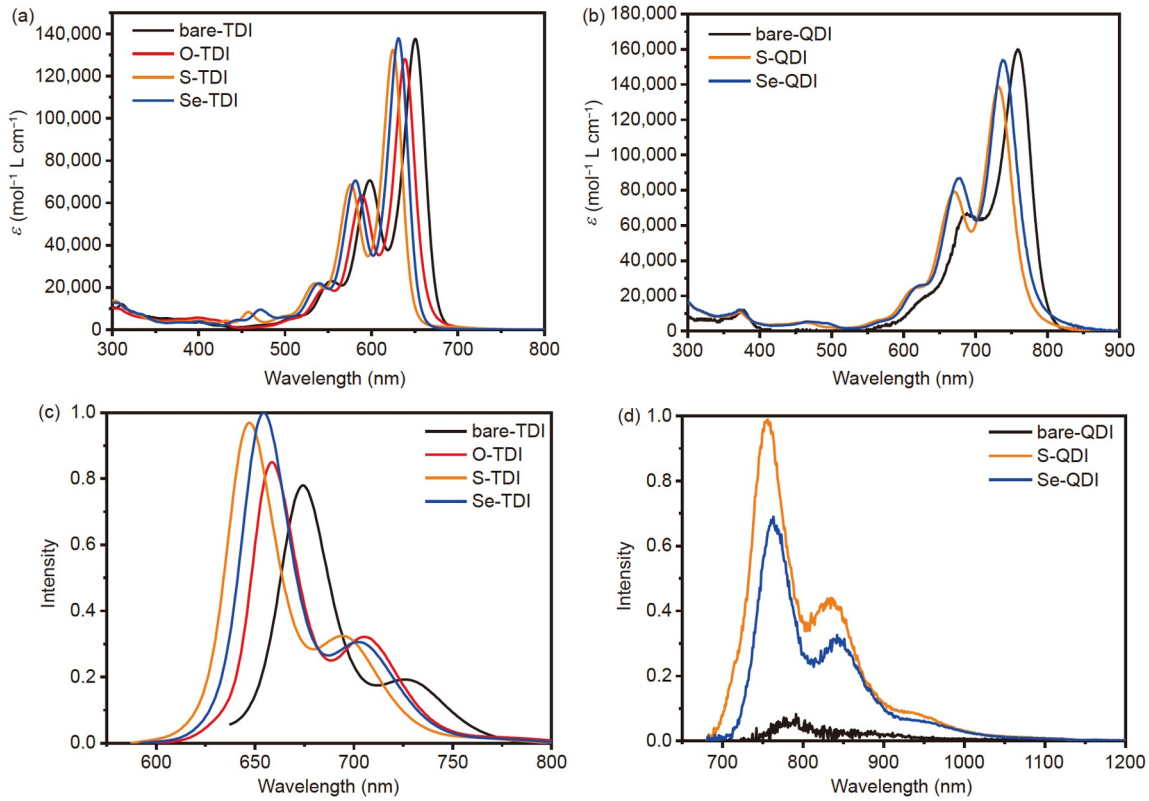

Figure 2 UV-vis-NIR absorption and fluorescence emission spectra of **bare-TDI**, **O-TDI**, **S-TDI**, **Se-TDI**, **bare-QDI**, **S-QDI** and **Se-QDI** in 10^{-5} mol L^{-1} toluene solution. The intensity of fluorescence is determined using the ratio of absolute Φ_{FL} (color online).

fluorescent brightness. The fluorescent brightness values of **bare-TDI**, **O-TDI**, **S-TDI**, and **Se-TDI** are 97,400, 100,900, 119,200, and 128,200 cm^{-1} mol^{-1} L, respectively. This consistent pattern of increasing Φ_{FL} and fluorescent brightness signifies a notable anti-heavy atom effect. To our best knowledge, this represents the first reported instance of the anti-heavy atom effect of chalcogens. The chalcogen-annulated **QDI** also show improvements in Φ_{FL} and fluorescent brightness. The Φ_{FL} of **bare-QDI**, **S-QDI**, and **Se-QDI** was measured to be 1%, 10%, and 7% (Table 1), respectively. The corresponding maximal ε values of **bare-QDI**, **S-QDI**, and **Se-QDI** are 172,700, 150,100, and 155,400 mol^{-1} L cm^{-1}, respectively. As a result, the fluorescent brightness of **bare-QDI**, **S-QDI**, and **Se-QDI** gradually increases to 1,700, 15,000, and 10,900 mol^{-1} L cm^{-1}, respectively.

Cyclic voltammetry (CV) measurements were performed in CH_2Cl_2 to investigate the electrochemical properties of the **TDI** and **QDI** fluorophores. The results, as shown in Table 1, Figures S1 and S2, reveal that both **TDI** and **QDI** fluorophores exhibit similar redox behavior characterized with one reversible oxidation wave and one reversible reduction wave. This indicates that the introduction of chalcogens to the **TDI** and **QDI** skeletons has negligible impact on their electrochemical properties. The half-wave reduction/oxidation potentials were −1.14/0.71 V for **bare-TDI**, −1.17/0.78 V for **O-TDI**, −1.19/0.76 V for **S-TDI**, −1.20/0.75 V for **Se-TDI**, −1.12/0.30 V for **bare-QDI**, −1.18/0.36 V for **S-QDI** and −1.17/0.39 V for **Se-QDI** *vs.* Fc/Fc^+. Therefore, the LUMO/HOMO/energy gap was determined to be −3.83/−5.36/1.53 eV for **bare-TDI**, −3.82/−5.41/1.59 eV for **O-TDI**, −3.82/−5.40/1.60 eV for **S-TDI**, −3.81/−5.38/1.57 eV for **Se-TDI**, −3.80/−5.00/1.20 eV for **bare-QDI**, −3.75/−5.04/1.29 eV for **S-QDI** and −3.74/−5.04/1.30 eV for **Se-QDI**.

2.3 Femtosecond transient absorption analysis and time-resolved fluorescence lifetime measurement

The excited-state dynamics of the **TDI** and **QDI** fluorophores were probed by femtosecond transient absorption (fs-TA) measurements in a toluene solution (0.2−0.3 OD at 595 nm for **bare-TDI** and **O-TDI**, 575 nm for **S-TDI**, 580 nm for **Se-TDI**, 667 nm for **bare-QDI**, **S-QDI** and **Se-QDI**). The spectral and kinetic components of the fs-TA spectra were analyzed by singular value decomposition analysis, followed by global analysis using the Glotaran program package [72]. The fs-TA spectra of **bare-TDI**, **O-TDI**, **S-TDI**, and **Se-TDI** in the initial few picoseconds after excitation display a negative ground-state bleach (GSB) and stimulated emission (SE) ranging from 500 to 750 nm (Figure 3a–3d) along with positive excited-state absorption (ESA) between 750 and 1,300 nm (Figure S3), correspond-

Table 1 Photophysical and electrochemical properties of **bare-TDI**, **O-TDI**,**S-TDI**, **Se-TDI**,**bare-QDI**, **S-QDI** and**Se-QDI**[a)]

Compound[a)]	$\lambda_{abs\ max}$ (nm)	ε (mol^{-1} L cm^{-1})	λ_{em} (nm)	Φ_{FL} [a),b)] (%)	B_F (mol^{-1} L cm^{-1})	E_{LUMO} [c),f)] (eV)	E_{HOMO} [c),f)] (eV)	E_g [d)] (eV)	τ_F (ns)	k_r [e)] (10^7 s^{-1})	k_{nr} [e)] (10^7 s^{-1})
Bare-TDI	650	135,300	667, 728	72	97,400	−3.83	−5.36	1.53	3.52	20.5	7.95
O-TDI	638	127,700	658, 710	79	100,900	−3.82	−5.41	1.59	3.64	21.7	5.77
S-TDI	624	132,400	638, 700	90	119,200	−3.82	−5.42	1.60	3.62	24.9	2.76
Se-TDI	631	137,800	645, 705	93	128,200	−3.81	−5.38	1.57	3.60	25.8	1.94
Bare-QDI	758	172,700	790, 860	1	1,700	−3.80	−5.00	1.20	0.45	2.22	220
S-QDI	731	150,100	766, 834	10	15,000	−3.75	−5.04	1.29	1.27	7.87	70.9
Se-QDI	737	155,400	775, 843	7	10,900	−3.74	−5.04	1.30	1.02	6.86	91.2

[a)] Measured in toluene (1.0×10^{-5} mol L^{-1}). [b)] Determined by absolute quantum yield method. [c)] Calculated by the onset of the first reduction peak according to E_{LUMO}=−(4.8+E^{re}_{onset}) eV, E_{HOMO}=(4.8+E^{ox}_{onset}) eV. [d)] E_g=E_{LUMO}−E_{HOMO}. [e)] The rates of radiative and nonradiative processes were determined by k_r=Φ_{FL}/τ_F and k_{nr}=(1−Φ_{FL})/τ_F. [f)] Measured in dichloromethane. B_F=fluorescent brightness.

ing to the singlet excited-state ($S_1\rightarrow S_n$; $n > 1$) of **bare-TDI**, **O-TDI**, **S-TDI** and **Se-TDI** [73]. The decay associated difference spectra (DADS) of each **bare-TDI**, **O-TDI**, **S-TDI** and **Se-TDI** were extracted (Figure 3e–3h). Three lifetimes (τ_1, τ_2, and τ_3) were extrapolated for **bare-TDI**, **S-TDI** and **Se-TDI**. Two lifetimes (τ_2, and τ_3) were extrapolated for **O-TDI**. Presumably, τ_1 (1.08, 5.48 and 6.65 ps for **bare-TDI**, **S-TDI** and **Se-TDI**, respectively) are assigned to the solvation or vibration-mediated relaxation to the lowest vibronic-state of the S_1, τ_2 (452, 262, 370 and 481 ps for **bare-TDI**, **O-TDI**, **S-TDI** and **Se-TDI**, respectively) corresponds to solvation of hot S_1 state as well as direct relaxation to the ground state from these higher vibrational S_1 state, and τ_3 (3.59, 3.34, 3.33 and 3.65 ns for **bare-TDI**, **O-TDI**, **S-TDI** and **Se-TDI**, respectively) corresponds to the decay of the lowest vibrational S_1 state to the ground-state. Meanwhile, the observed singlet lifetimes are comparable to the fluorescence lifetime of these molecules (3.53, 3.64, 3.62 and 3.60 ns for **bare-TDI**, **O-TDI**, **S-TDI** and **Se-TDI**, respectively, as shown in Table 1 and Figure S4.

The excited-state dynamics of **QDI** fluorophores are very similar to that of **TDI** fluorophores. The longest excited-state lifetimes of **bare-QDI**, **S-QDI** and **Se-QDI** are 0.28, 1.21 and 1.49 ns (Figure S5), respectively, and the excited-state lifetimes are also comparable to the fluorescence lifetimes (0.45, 1.27 and 1.02 ns for **bare-QDI**, **S-QDI** and **Se-QDI**, respectively, as shown in Table 1 and Figure S6). Based on the fs-TA and time-resolved fluorescence lifetime experiments, it can be concluded that ISC process is negligible in the **TDI** and **QDI** fluorophores, that is, the presence of heavy atoms does not accelerate the process of ISC.

2.4 Theoretical calculations

To investigate the reason of enhancing the Φ_{FL} and fluorescent brightness of **TDI** and **QDI** fluorophores, we conducted comprehensive theoretical calculations to thoroughly investigate the effect of annulation of chalcogens on these processes. The rate of intersystem crossing (k_{ISC}) is influenced by two crucial factors: the energy gap between the singlet- and triplet-states (ΔE_{ST}), and the total spin–orbit coupling matrix elements (H_{SOC}) [74]. According to perturbation theory, k_{ISC} between singlet (S_m) and triplet (T_n) states is proportional to the square of their H_{SOC}. And according to the energy gap law, k_{ISC} is exponentially related to their ΔE_{ST} (equation 1). The oscillator strength of singlet transitions confirms that the $S_0 \rightarrow S_1$ transition is the most probable in **TDI** fluorophores (Table S1 and S2). Additionally, the T_3 state is too high in energy to be reached in room temperature (Table S2 and S3). Therefore, the $S_1 \rightarrow T_1$ and $S_1 \rightarrow T_2$ transition may have the most significant impact on k_{ISC}. We employed the molecular materials property prediction package (MOMAP) [75–78] to calculate the rates of transitions from S_1 to S_0, T_1 and T_2.

As shown in Table 2, the fluorescence rates of **bare-TDI** and chalcogen-annulated **TDI** are significantly larger than the internal conversion rates, leading to high Φ_{FL}. The calculated rates of fluorescence (k_F, also called k_r) exhibit an approximate 25% increase from **bare-TDI** to **O-TDI**, **S-TDI**, and **Se-TDI**, aligning with experimental trends. Considering the nearly identical oscillator strengths among the four molecules (Table S2) and minimal differences in S_1–S_0 energy gaps, it seems that changes in vibrational properties contribute to the increase in k_F. However, this observed increase remains marginal, and conducting a comprehensive analysis to ascertain the precise underlying causes of the enhanced Φ_{FL} remains challenging.

On the other hand, the intersystem crossing rates are all negligible in **TDI** fluorophores. The large energy gap and negligible spin–orbital coupling matrix element between S_1 and T_1 make the $S_1 \rightarrow T_1$ transition very slow. Meanwhile, the transition from $S_1 \rightarrow T_2$ is also negligible, being very different from previously reported **PDI** systems [37]. The annulation of chalcogens in **TDI** fluorophores does not considerably alter the energy gap between S_1 and T_2 states, and the difference is higher than 0.25 eV in **bare-TDI**, **O-**

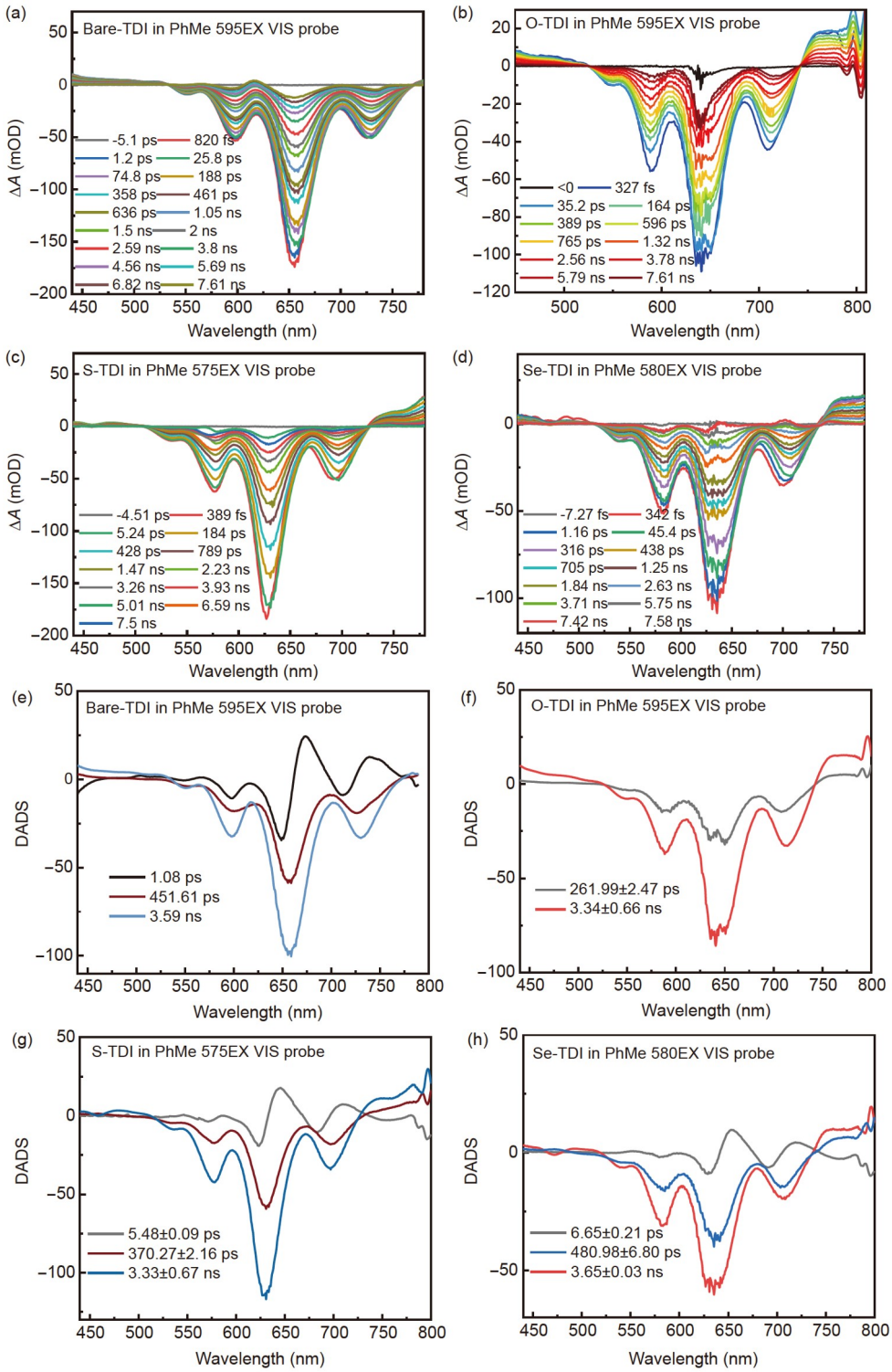

Figure 3 Femtosecond transient absorption spectra of (a) **bare-TDI**, (b) **O-TDI**, (c) **S-TDI** and (d) **Se-TDI** in toluene. Reconstructed decay-associated difference spectra (DADS) of (e) **bare-TDI**, (f) **O-TDI**, (g) **S-TDI** and (h) **Se-TDI** extracted from global analysis (color online).

TDI, **S-TDI**, and **Se-TDI**. Generally, energy barriers that can be crossed at room temperature are usually below 0.2 eV. As a result, the transition from S_1 to T_2 in **TDI** fluorophores is nearly forbidden. Furthermore, the H_{SOC} of **TDI** fluorophores is less than 0.1 cm^{-1}. The high ΔE_{ST} and very low H_{SOC} result in the inhibition of ISC (Table 2).

$$k_{ISC} \propto \left|\langle S_m|\widehat{H}_{SOC}|T_n\rangle\right|^2 \exp(-\Delta E / kT) \quad (1)$$

To further analyze why ΔE_{ST} and H_{SOC} of chalcogen-annulated **TDI** and **QDI** do not increase with the atomic

number of O, S, and Se, we conducted calculations of electron density changes in the excited-states of each molecule and generated charge density difference (CDD) data and plots (Figure 4, Figures S7 and S8, Table 2 and Table S1) [79–81]. The contribution ratio of CDD from O, S, and Se atoms in chalcogen-annulated **TDI** is provided in Table 2 and Figure 4. It is evident that the CDD of S_1 and T_2 states in the chalcogen-annulated **TDI** primarily distributes on the conjugated skeleton. The contribution of O, S, and Se atoms to the excited S_1 (1.37, 2.56 and 2.81% for O, S and Se) and T_2 state (0.92, 0.54 and 2.19% for O, S and Se) is minimal and there is no significant change in CDD near the O, S, and Se atoms. Chalcogen-annulated **QDI** exhibit similar CDD data as chalcogen-annulated **TDI** (Table S1 and Figure S7), the S and Se atomic orbitals do not play a significant role in the $S_1 \rightarrow T_2$ transition process of chalcogen-annulated **QDI**. Consequently, we can conclude that the annulation of chalcogens does not significantly impact the properties of S_1 and T_2 states in chalcogen-annulated **TDI** and **QDI**, leading to negligible changes in $\Delta E_{S_1-T_2}$ and $H_{SOC\ S_1-T_2}$.

It is noteworthy that we also calculated the CDD of chalcogen-annulated **PDI**, as depicted in Figure S8 and Table S1. We observe substantial contributions of S and Se to the CDD of chalcogen-annulated **PDI** at T_2 state, reaching 31.5% and 42.5%, respectively. The high CDD of S and Se atoms leads to a significant reduction in the energy of the T_2 state (reflected by the decrease of $\Delta E_{S_1-T_2}$) and an increase in the H_{SOC} of $S_1 \rightarrow T_2$ transition. Consequently, the k_{ISC} in chalcogen-annulated **PDI** is significantly enhanced. These findings are supported by previous reports where chalcogen-annulated **PDI** follows the heavy-atom effect [37]. The CDD calculations provide a plausible explanation for the distinct fluorescence properties of chalcogen-annulated **PDI** with chalcogen-annulated **TDI** and **QDI**.

Interestingly, the internal conversion rates experience a substantial decrease by several folds. To investigate the impact of chalcogen-annulation on the IC process (the non-radiative transition from S_1 to S_0), we analyzed the ground-state reorganization energy of **bare-TDI**, **O-TDI**, **S-TDI**, and **Se-TDI**. The calculation results from MOMAP indicate negligible variation in the total reorganization energy of 769.0, 774.4, 790.3, and 783.2 cm^{-1} for **bare-TDI**, **O-TDI**, **S-TDI**, and **Se-TDI**, respectively. However, the annulation of chalcogens enhances the rigidity of the annulative region and disrupts the molecular symmetry. This case leads to the dispersion of the large reorganization energy in **bare-TDI** into multiple smaller reorganization energies in **O-TDI**, **S-TDI**, and **Se-TDI**, leading to gradual decrease of the large reorganization energy in **bare-TDI, O-TDI**, **S-TDI**, and **Se-TDI** (255.56, 212.64, 157.58 and 148.44 cm^{-1}, respectively), and as a result, gradually decreasing the rate of IC in **bare-TDI, O-TDI**, **S-TDI**, and **Se-TDI** (Table 2).

A more specific analysis is as shown in Figure 5a. In **bare-TDI**, the vibrational modes at 1,318 cm^{-1} and 1,611 cm^{-1}

Table 2 Calculated energies of S_1, T_1, T_2, ΔE_{ST}, H_{SOC}, k_{ISC} values of $S_1 \rightarrow T_1$ and $S_1 \rightarrow T_2$ transition, fluorescence rate (k_F) and internal conversion rate (k_{IC}) of $S_1 \rightarrow S_0$ transition, in **Bare-TDI**, **O-TDI**, **S-TDI**, and **Se-TDI**. The contribution of oxygen, sulfur and selenium atoms to CDD is also given. All energies in eV, except H_{SOC} in cm^{-1}. Rates in s^{-1}

Compound	S_1	T_1	T_2	ΔE_{ST} S_1–T_2	H_{SOC} S_1–T_2	CDD X%S_1	CDD X%T_2	k_F S_1–S_0	k_{IC} S_1–S_0	k_{ISC} S_1–T_1 [a)]	k_{ISC} S_1–T_2
Bare-TDI	1.61	0.52	1.86	0.25	0.005	/	/	1.30×10^{8}	4.10×10^{6}	9.13×10^{-5}	1.53×10^{-1}
O-TDI	1.69	0.65	1.95	0.26	0.085	1.37	0.92	1.29×10^{8}	8.00×10^{5}	3.08×10^{-2}	3.06×10^{2}
S-TDI	1.71	0.71	1.96	0.25	0.087	2.56	0.54	1.55×10^{8}	6.09×10^{5}	2.90×10^{-3}	4.33×10^{2}
Se-TDI	1.70	0.70	1.95	0.25	0.092	2.81	2.19	1.50×10^{8}	7.49×10^{5}	0	3.57×10^{2}

[a)] The Fermi golden rule may not be accurate for slow process such as the k_{ISC} of S_1–T_1, but it is certain that they are negligible.

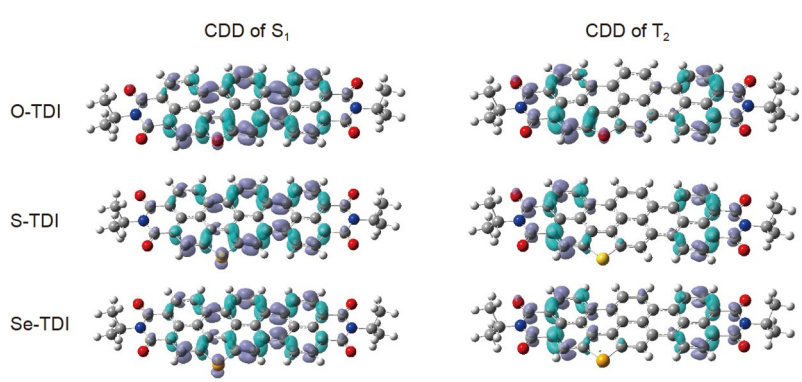

Figure 4 Charge density difference (CDD) plots of chalcogen-annulated **TDI** at S_1 and T_2 states at (TD-)B3LYP(GD3BJ)/def2svp level, the cyan represents the main distribution area of CDD (color online).

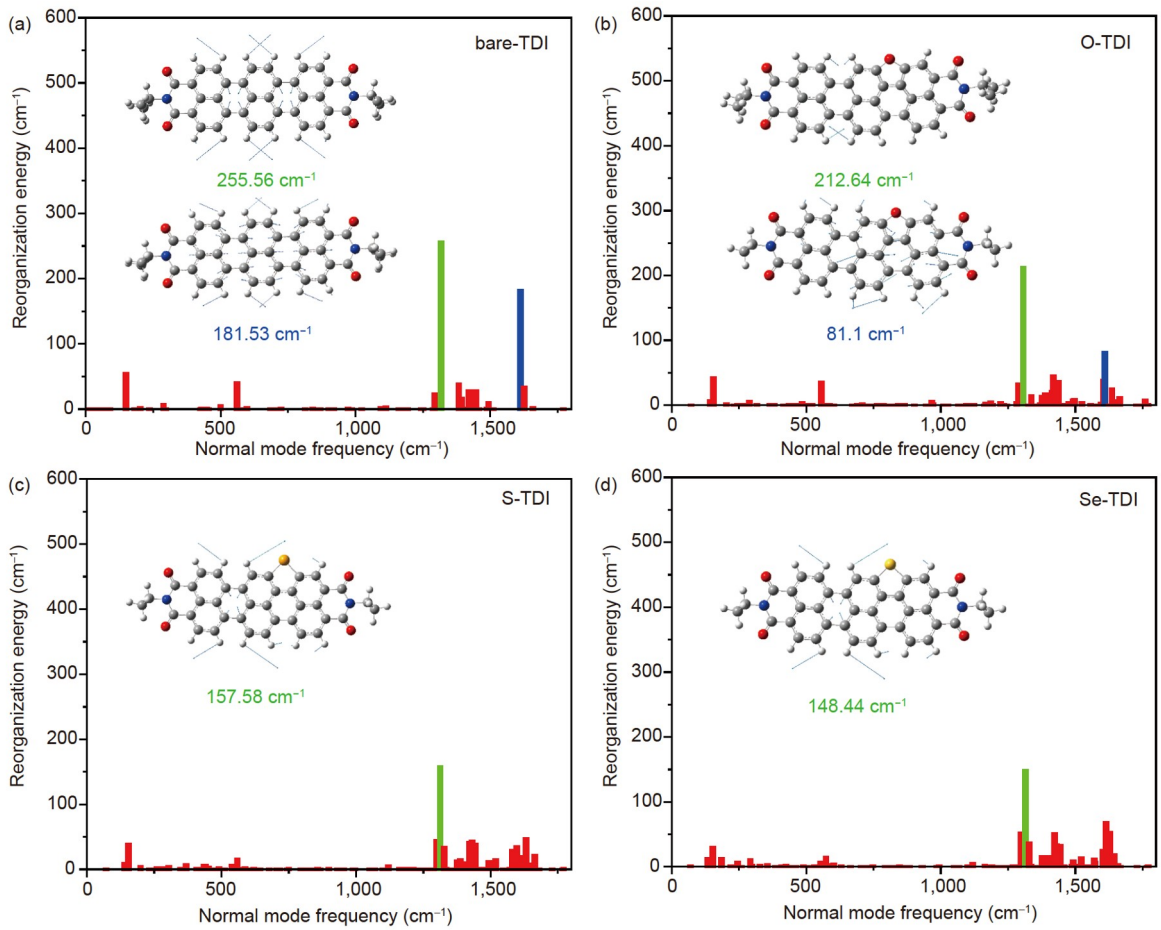

Figure 5 Calculated reorganization energies of $S_1 \rightarrow S_0$ are plotted against the normal-mode frequencies of (a) **bare-TDI**, (b) **O-TDI**, (c) **S-TDI** and (d) **Se-TDI**. High-intensity (>80 cm^{-1}) vibrational modes are shown as inset (color online).

have the highest reorganization energy, with values of 255.56 cm^{-1} and 181.53 cm^{-1}, respectively. They can be interpreted as longitudinal and transverse stretching vibrations of the two bridged benzene rings (Figure 5a inset). In **O-TDI**, the vibrational mode at 1,318 cm^{-1} changes to asymmetric longitudinal stretching vibrations primarily associated with the left hand-side benzene rings (upper inset of Figure 5b), while the right hand-side annulative region exhibits minimal vibration. Consequently, the reorganization energy of the vibrational mode at 1,318 cm^{-1} decreases from 255.56 cm^{-1} in **bare-TDI** to 212.64 cm^{-1} in **O-TDI**. The vibrational mode at 1,611 cm^{-1} splits into three vibrational modes of 1,605.9, 1,609.9 and 1,664.3 cm^{-1} in **O-TDI,** and the highest reorganization energy of the vibrational mode nearby 1,611 cm^{-1} also changes from 181.53 cm^{-1} in **bare-TDI** to 81.1 cm^{-1} in **O-TDI** (under inset of Figure 5b). This phenomenon becomes even more pronounced in **S-TDI** and **Se-TDI**, where the reorganization energy of these accepting modes at ground-state is 157.58 cm^{-1} and 148.44 cm^{-1}, respectively (Figure 5c and 5d). Overall, the chalcogen-annulation of **TDI** fluorophores with the progressive decrease in reorganization energy of several most important accepting modes in the ground-state effectively suppresses the likelihood of IC from S_1 to S_0. This inhibition becomes more pronounced with the increase in atomic number of the chalcogens (**O-TDI** < **S-TDI** < **Se-TDI**).

3 Conclusions

In summary, we demonstrated a straightforward and effective chalcogen-annulation strategy to enhance the deep-red/near-infrared Φ_{FL} and fluorescent brightness of **QDI** and **TDI** fluorophores. The Φ_{FL} of **S-QDI** and **Se-QDI** is 10%, and 7% and their fluorescent brightness values are 15,000, and 10,900 cm^{-1} mol^{-1} L. These values represent a tenfold enhancement compared with those of **bare-QDI** (Φ_{FL} = 1%, and fluorescent brightness = 1,700 cm^{-1} mol^{-1} L). The Φ_{FL} (72%, 79%, 90% and 93%) and the fluorescent brightness (97,400, 109,000, 119,200, and 128,200 cm^{-1} mol^{-1} L) of **bare-TDI**, **O-TDI**, **S-TDI**, and **Se-TDI**, respectively, demonstrate a progressive increase. The continuous enhancement of Φ_{FL} and fluorescent brightness of **TDI** fluorophores exhibits the first example of the anti-heavy-atom effect of

chalcogens and the Φ_{FL} (93%) and fluorescent brightness (128,200 cm^{-1} mol^{-1} L) of **Se-TDI** is among the top of currently available deep-red/near-infrared fluorophores. The detailed mechanism is depicted in Figure 1c. The high energy gap and low H_{SOC} between the $S_1 \rightarrow T_1$ and $S_1 \rightarrow T_2$ indicate a negligible ISC rate in **TDI** fluorophores (the cyan squiggly arrow in Figure 1c). The chalcogen-annulation-induced alteration in vibrational properties potentially leads to a gradual increase in radiative rates within **TDI** fluorophores (green, orange, blue and red straight arrows in Figure 1c, respectively). Additionally, the decrease of the highest reorganization energy in the ground-states across **bare-TDI**, **O-TDI**, **S-TDI**, and **Se-TDI** (green, orange, blue and red squiggly arrows in Figure 1c, respectively) reduces the rate of IC in **TDI** fluorophores. Our chalcogen-annulation strategy provides valuable insights and theoretical supports for designing and synthesizing novel deep-red/near-infrared organic fluorophores with high Φ_{FL} and brightness. The synthesis of chalcogen-annulated pentarylene- and hexarylene diimide fluorophores with high near-infrared-II fluorescence is ongoing in our laboratory.

Acknowledgements This work was financially supported by the National Natural Science Foundation of China (NSFC) (22235005), the National Postdoctoral Program for Innovative Talents (BX20200128), the 69th batch of Chinese postdoctoral general support (2021M691004), Shanghai Municipal Science and Technology Major Project (2018SHZDZX03) and the Fundamental Research Funds for the Central Universities, the Programme of Introducing Talents of Discipline to Universities (B16017). We acknowledge Prof. He Tian from East China University of Science and Technology for the constructive guidance.

Conflict of interest The authors declare no conflict of interest.

Supporting information The supporting information is available online at chem.scichina.com and link.springer.com/journal/11426. The supporting materials are published as submitted, without typesetting or editing. The responsibility for scientific accuracy and content remains entirely with the authors.

1 Weissleder R, Pittet MJ. *Nature*, 2008, 452: 580–589
2 Gigan S. *Nat Photon*, 2017, 11: 14–16
3 Li C, Chen G, Zhang Y, Wu F, Wang Q. *J Am Chem Soc*, 2020, 142: 14789–14804
4 Wei YC, Kuo KH, Chi Y, Chou PT. *Acc Chem Res*, 2023, 56: 689–699
5 Chen X, Pradhan T, Wang F, Kim JS, Yoon J. *Chem Rev*, 2012, 112: 1910–1956
6 Li X, Gao X, Shi W, Ma H. *Chem Rev*, 2014, 114: 590–659
7 Ando N, Soutome H, Yamaguchi S. *Chem Sci*, 2019, 10: 7816–7821
8 Wei R, Dong Y, Wang X, Li J, Lei Z, Hu Z, Chen J, Sun H, Chen H, Luo X, Qian X, Yang Y. *J Am Chem Soc*, 2023, 145: 12013–12022
9 Li H, Kim H, Xu F, Han J, Yao Q, Wang J, Pu K, Peng X, Yoon J. *Chem Soc Rev*, 2022, 51: 1795–1835
10 Gorka AP, Nani RR, Schnermann MJ. *Acc Chem Res*, 2018, 51: 3226–3235
11 Sun W, Guo S, Hu C, Fan J, Peng X. *Chem Rev*, 2016, 116: 7768–7817
12 Zhou HJ, Ren TB. *Chem An Asian J*, 2022, 17: e202200147
13 Lu H, Mack J, Yang Y, Shen Z. *Chem Soc Rev*, 2014, 43: 4778–4823
14 Yuan L, Lin W, Zheng K, He L, Huang W. *Chem Soc Rev*, 2013, 42: 622–661
15 Kamkaew A, Lim SH, Lee HB, Kiew LV, Chung LY, Burgess K. *Chem Soc Rev*, 2013, 42: 77–88
16 Zhao X, Zhang F, Lei Z. *Chem Sci*, 2022, 13: 11280–11293
17 Zhao J, Xu K, Yang W, Wang Z, Zhong F. *Chem Soc Rev*, 2015, 44: 8904–8939
18 Cao D, Liu Z, Verwilst P, Koo S, Jangjili P, Kim JS, Lin W. *Chem Rev*, 2019, 119: 10403–10519
19 Iglesias-Artola JM, Nadler A. *Acc Chem Res*, 2023, 56: 810–820
20 Chen Y, Chen S, Yu H, Wang Y, Cui M, Wang P, Sun P, Ji M. *Adv Healthcare Mater*, 2022, 11: e2201158
21 Neto BAD, Carvalho PHPR, Correa JR. *Acc Chem Res*, 2015, 48: 1560–1569
22 Xu Z, Jiang Y, Fan M, Tang S, Liu M, Law WC, Yang C, Ying M, Ma M, Dong B, Yong KT, Xu G. *Adv Opt Mater*, 2021, 9: 2100859
23 Mu J, Xiao M, Shi Y, Geng X, Li H, Yin Y, Chen X. *Angew Chem Int Ed*, 2022, 61: e202114722
24 Liu Y, Hao A, Xing P. *Sci China Chem*, 2023, 66: 2130–2140
25 Englman R, Jortner J. *Mol Phys*, 1970, 18: 145–164
26 Jiang W, Li Y, Wang Z. *Acc Chem Res*, 2014, 47: 3135–3147
27 Liang N, Meng D, Wang Z. *Acc Chem Res*, 2021, 54: 961–975
28 Jiang W, Wang Z. *J Am Chem Soc*, 2022, 144: 14976–14991
29 Zhan X, Facchetti A, Barlow S, Marks TJ, Ratner MA, Wasielewski MR, Marder SR. *Adv Mater*, 2011, 23: 268–284
30 Bialas D, Kirchner E, Röhr MIS, Würthner F. *J Am Chem Soc*, 2021, 143: 4500–4518
31 Würthner F, Saha-Möller CR, Fimmel B, Ogi S, Leowanawat P, Schmidt D. *Chem Rev*, 2016, 116: 962–1052
32 Schmaltz B, Weil T, Müllen K. *Adv Mater*, 2009, 21: 1067–1078
33 Ball M, Zhang B, Zhong Y, Fowler B, Xiao S, Ng F, Steigerwald M, Nuckolls C. *Acc Chem Res*, 2019, 52: 1068–1078
34 Weil T, Vosch T, Hofkens J, Peneva K, Müllen K. *Angew Chem Int Ed*, 2010, 49: 9068–9093
35 Young RM, Wasielewski MR. *Acc Chem Res*, 2020, 53: 1957–1968
36 Harvey SM, Wasielewski MR. *J Am Chem Soc*, 2021, 143: 15508–15529
37 Sivanarayanan J, Sebastian E, Vinod K, Würthner F, Hariharan M. *J Phys Chem C*, 2022, 126: 13319–13326
38 Hu YX, Miao J, Hua T, Huang Z, Qi Y, Zou Y, Qiu Y, Xia H, Liu H, Cao X, Yang C. *Nat Photon*, 2022, 16: 803–810
39 Cao X, Pan K, Miao J, Lv X, Huang Z, Ni F, Yin X, Wei Y, Yang C. *J Am Chem Soc*, 2022, 144: 22976–22984
40 Huang Z, Xie H, Miao J, Wei Y, Zou Y, Hua T, Cao X, Yang C. *J Am Chem Soc*, 2023, 145: 12550–12560
41 Wang Z, Sun Y, Lin S, Wang G, Chang X, Gou X, Liu T, Jin S, He G, Wei YC, Chou PT, Fang Y. *Sci China Chem*, 2021, 64: 2193–2202
42 Wu Y, Liu Y, Jiang W, Wang Z. *Sci China Chem*, 2023, 66: 2400–2407
43 Liu G, Liu Y, Zhao C, Li Y, Wang Z, Tian H. *Angew Chem Int Ed*, 2023, 62: e202214769
44 Powell D, Whittaker-Brooks L. *Mater Horiz*, 2022, 9: 2026–2052
45 Bao ST, Jiang H, Jin Z, Nuckolls C. *Chirality*, 2023, 35: 656–672
46 Renner R, Stolte M, Heitmüller J, Brixner T, Lambert C, Würthner F. *Mater Horiz*, 2022, 9: 350–359
47 Sun M, Müllen K, Yin M. *Chem Soc Rev*, 2016, 45: 1513–1528
48 Ashoka AH, Aparin IO, Reisch A, Klymchenko AS. *Chem Soc Rev*, 2023, 52: 4525–4548
49 Chen S, Zhou M, Zhu L, Yang X, Zang L. *Chemosensors*, 2023, 11: 293
50 Chen Y. *Molecules*, 2022, 27: 8628
51 Herrmann A, Müllen K. *Chem Lett*, 2006, 35: 978–985
52 Pschirer NG, Kohl C, Nolde F, Qu J, Müllen K. *Angew Chem Int Ed*, 2006, 45: 1401–1404
53 Ji C, Cheng W, Yuan Q, Müllen K, Yin M. *Acc Chem Res*, 2019, 52: 2266–2277
54 Mahlmeister B, Mahl M, Reichelt H, Shoyama K, Stolte M, Würthner

F. *J Am Chem Soc*, 2022, 144: 10507–10514
55 Hu W, Prasad PN, Huang W. *Acc Chem Res*, 2021, 54: 697–706
56 Mehra KS, Jha S, Bhandary S, Mandal D, Mishra R, Sankar J. *Angew Chem Int Ed*, 2022, 61: e202205600
57 Cruz CM, Walsh JC, Juríček M. *Org Mater*, 2022, 4: 163–169
58 Chen M, Krzyaniak MD, Nelson JN, Bae YJ, Harvey SM, Schaller RD, Young RM, Wasielewski MR. *Proc Natl Acad Sci USA*, 2019, 116: 8178–8183
59 Pan HM, Wu CC, Lin CY, Hsu CS, Tsai YC, Chowdhury P, Wang CH, Chang KH, Yang CH, Liu MH, Chen YC, Su SP, Lee YJ, Chiang HK, Chan YH, Chou PT. *J Am Chem Soc*, 2023, 145: 516–526
60 Penfold TJ, Gindensperger E, Daniel C, Marian CM. *Chem Rev*, 2018, 118: 6975–7025
61 Steffen A, Tay MG, Batsanov AS, Howard JAK, Beeby A, Vuong KV, Sun XZ, George MW, Marder T . *Angew Chem Int Ed*, 2010, 49: 2349–2353
62 Tong GSM, Chow PK, Che CM. *Angew Chem Int Ed*, 2010, 49: 9206–9209
63 Eng J, Gourlaouen C, Gindensperger E, Daniel C. *Acc Chem Res*, 2015, 48: 809–817
64 Yan X, Cook TR, Wang P, Huang F, Stang PJ. *Nat Chem*, 2015, 7: 342–348
65 Cannizzo A, Blanco-Rodríguez AM, El Nahhas A, Šebera J, Záliš S, Vlček Jr. A, Chergui M. *J Am Chem Soc*, 2008, 130: 8967–8974
66 Wei YC, Chen BH, Ye RS, Huang HW, Su JX, Lin CY, Hodgkiss J, Hsu LY, Chi Y, Chen K, Lu CH, Yang SD, Chou PT. *Angew Chem Int Ed*, 2023, 62: e202300815
67 Boulanger SA, Chen C, Tang L, Zhu L, Baleeva NS, Myasnyanko IN, Baranov MS, Fang C. *Phys Chem Chem Phys*, 2021, 23: 14636–14648
68 Xu P, Qiu Q, Ye X, Wei M, Xi W, Feng H, Qian Z. *Chem Commun*, 2019, 55: 14938–14941
69 Mayerhöffer U, Fimmel B, Würthner F. *Angew Chem Int Ed*, 2012, 51: 164–167
70 Wu J, Shi Z, Zhu L, Li J, Han X, Xu M, Hao S, Fan Y, Shao T, Bai H, Peng B, Hu W, Liu X, Yao C, Li L, Huang W. *Adv Opt Mater*, 2022, 10: 2102514
71 Mehra KS, Jha S, Menon AM, Chopra D, Sankar J. *Chem Sci*, 2023, 14: 3147–3153
72 van Stokkum IHM, Larsen DS, van Grondelle R. *Biochim Biophys Acta (BBA) - Bioenergetics*, 2004, 1657: 82–104
73 Margulies EA, Miller CE, Wu Y, Ma L, Schatz GC, Young RM, Wasielewski MR. *Nat Chem*, 2016, 8: 1120–1125
74 Sasikumar D, John AT, Sunny J, Hariharan M. *Chem Soc Rev*, 2020, 49: 6122–6140
75 Niu Y, Li W, Peng Q, Geng H, Yi Y, Wang L, Nan G, Wang D, Shuai Z. *Mol Phys*, 2018, 116: 1078–1090
76 Niu YL, Peng Q, Shuai ZG. *Sci China Ser B-Chem*, 2008, 51: 1153–1158
77 Shuai Z. *Chin J Chem*, 2020, 38: 1223–1232
78 Peng Q, Yi Y, Shuai Z, Shao J. *J Am Chem Soc*, 2007, 129: 9333–9339
79 Liu Z, Lu T, Chen Q. *Carbon*, 2020, 165: 461–467
80 Zhu G, Chen Z, Song H, You A, Li Z. *RSC Adv*, 2022, 12: 18238–18244
81 Shi YH, Wang F, Sun GY, Xie YZ. *SpectroChim Acta Part A-Mol Biomol Spectr*, 2022, 264: 120249